ADVANCED FUNCTIONAL MATERIALS

Supporting Information

for *Adv. Funct. Mater.,* DOI: 10.1002/adfm.201601353

Multistability in Bistable Ferroelectric Materials toward Adaptive Applications

Anirban Ghosh, Gertjan Koster, and Guus Rijnders*

WILEY-VCH

Supplementary Information

Multi-stability in bi-stable ferroelectric materials towards adaptive applications

Anirban Ghosh, Gertjan Koster and Guus Rijnders*

Mr. Anirban Ghosh, Prof. Gertjan Koster* and Prof. Guus Rijnders

Faculty of Science and Technology and MESA+ Institute for Nanotechnology, University Twente, P.O. Box 217, 7500AE Enschede, The Netherlands

E-mail: G.Koster@utwente.nl

Keywords: (Ferroelectrics, Adaptive application, Multi-state memory, Switching dynamics, Statistics of switching)

1. Neuron Activation Functions

Activation functions can be broadly classified as hard and soft activation functions. For realizing a discreet neuron (perceptron) a hard activation function is used based on ON and OFF switch, this can be used to solve simple problems very fast however the convergence might not be accurate and are only be used as binary classifiers. For more complex, continuous neurons (multi-layer perceptrons) where learning and accuracy are most important one needs soft activation functions which are generally sigmoidal. The ability of a neural network to learn depends on the number of degrees of freedom available to the network (for an electronic device it means the number of switchable states). The number of degrees of freedom determines the plasticity of the system, i.e., its capability of approximating the training set (plasticity scales with the number of degrees of freedom) [1-9]. For a rapid convergence and avoiding over shooting the weights need to be adjusted gradually in small steps and which requires a moderate slope of the activation function. In general the lesser the slope of the polarization switching curve higher will be the plasticity which in turn enhances the learning ability and helps to reduce the training error [7, 9, 10].

2. Structural characterizations

a) X-ray diffraction

The crystallographic properties of the aforementioned heterostructure were investigated by X-Ray diffraction (XRD) (Panalytical X'Pert Powder diffractometer and X'Pert MRD). **Figure. S1** (a) shows the XRD spectrum of device PZT100, showing the epitaxial (111) growth of PZT and SRO. **Figure. S1** (b) shows the XRD spectrum of the heterostructure around the (321) reflections. The reciprocal space map around (321) and (111) reflections showed that the PZT was rhombohedral with lattice constant of 4.08 Å. We note from the reciprocal space map that the PZT films are fully relaxed.

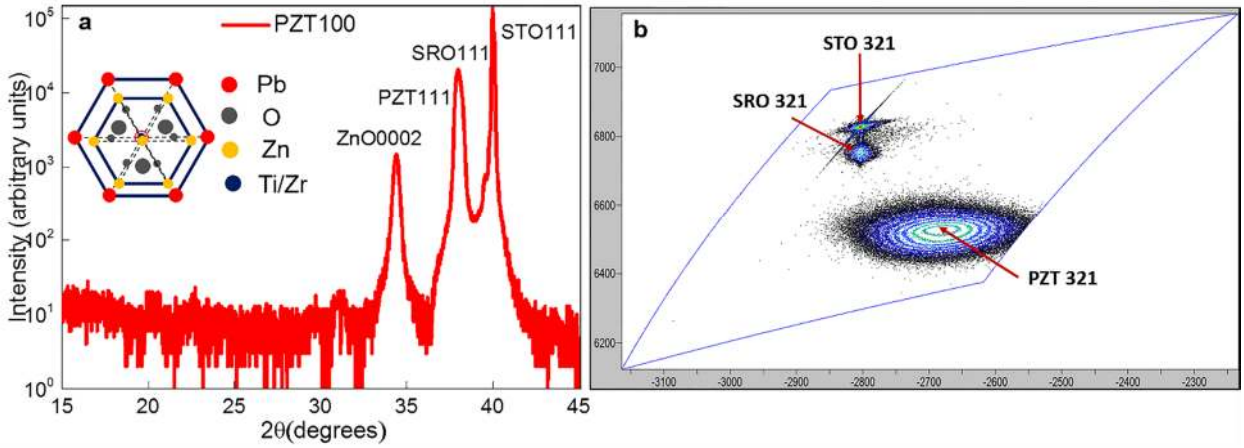

Figure. S1 (a) **Figure. S1** (b)

Figure. S1 (a) The X-ray diffraction spectrum θ-2θ scan of the PZT100 heterostructure around the (111) reflections. (b) The reciprocal space map of the heterostructure around the (321) reflections of the heterostructure.

b) Atomic force microscopy

The surface roughness of the structures were measured using a Bruker Icon AFM. Different thicknesses of ZnO were grown on a thin layer of SRO (10 nm)/ PZT (10 nm) to find the roughness of the ZnO layers. The average rms roughness of the SRO/PZT layer was 2 nm over an area of 5µm × 5µm. The rms roughness of the ZnO layer was 4 nm and was almost invariant with the thickness of ZnO.

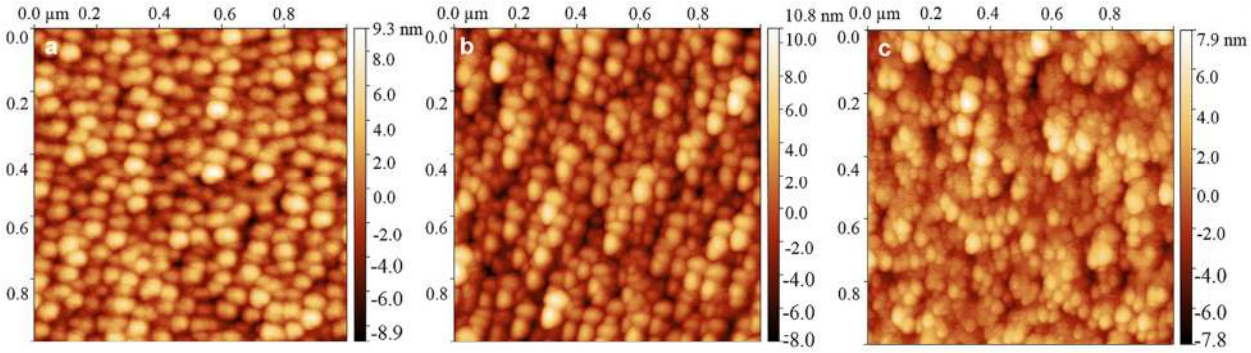

Figure. S2 (a) **Figure. S2** (b) **Figure. S2** (c)

Figure. S2 AFM topography scans of the surface of (a) 25 nm ZnO (b) 50 nm ZnO and (c) 100 nm ZnO films used in our studies, showing a root-mean-square roughness of ~ 4 nm

c) Transmission electron microscopy

The local structure and interface layer was probed using a Philips CM300ST FEG Transmission electron microscope (TEM). The TEM images showed sharp PZT-ZnO interfaces with no signs of inter-diffusion. Fast Fourier transform of the images showed that the PZT was oriented along the [111] direction and ZnO along the [0001] direction.

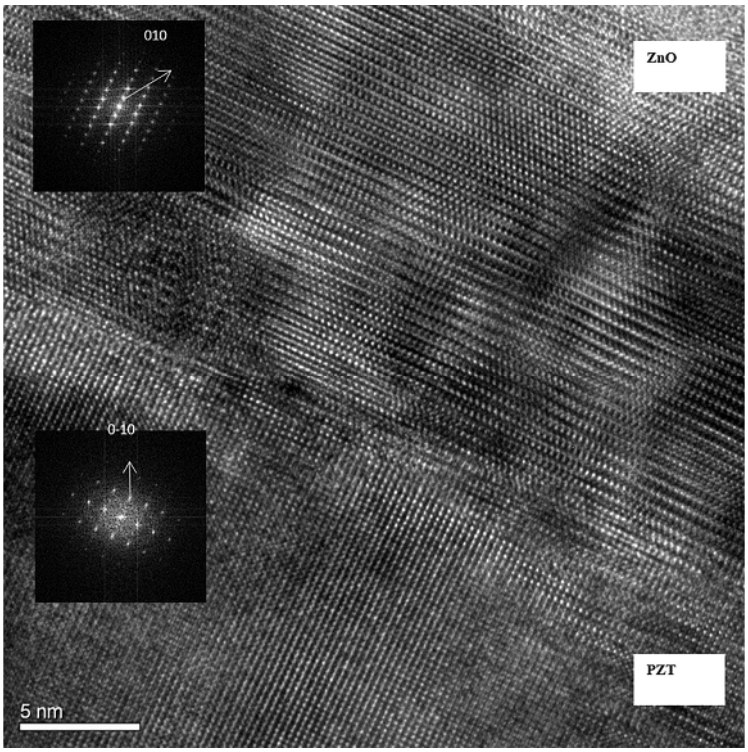

Figure. S3

Figure. S3. Cross-section TEM image of the PZT-ZnO interface PZT100 epitaxial film, the insets show the fast Fourier transform of the image.

3. Electrical Measurements

a) Ferroelectric Hysteresis

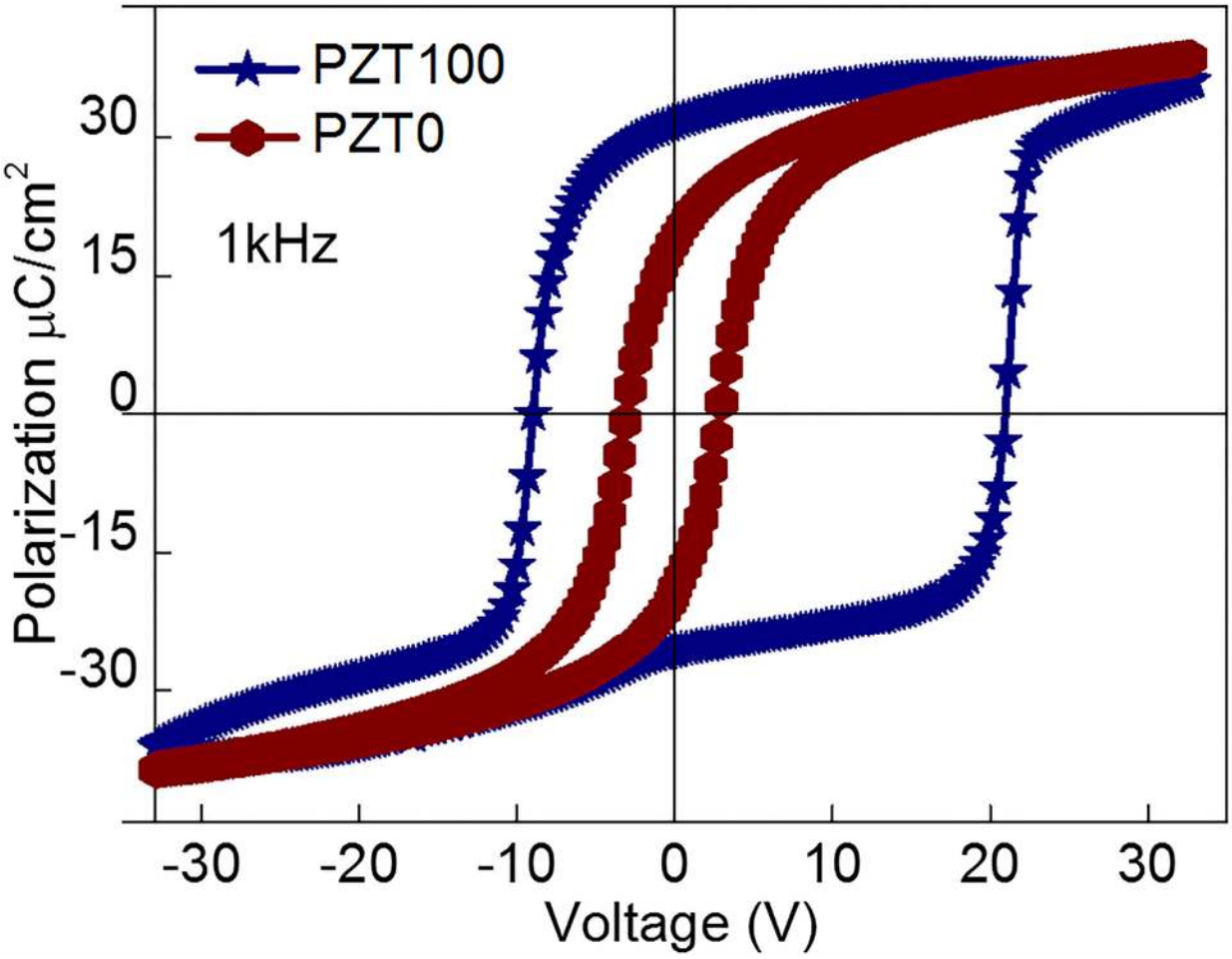

Figure. S4

Figure. S4 Ferroelectric P-V hysteresis loop measured at 1 kHz of the PZT0 and PZT100 samples

Ferroelectric characterizations were carried out at room temperature using an aixACCT 3000 TF Analyzer set up. In order to measure the tuning of the ferroelectric hysteresis with the ZnO thickness we measured the P-V hysteresis loop for the four different thicknesses of ZnO along with PZT without any ZnO. In **Figure. S4** we show the P-V hysteresis loops of the PZT0 and PZT100 devices measured at 1 kHz. The coercive voltage was independent of the measurement frequency (10 Hz-10 kHz) to a first order approximation. Typically the defect dynamics involving charging/discharging of the defect states and presence of electrets result in large frequency dispersion of the hysteresis loops in ferroelectrics[11-13]. This shows that our electrical measurements are not dominated by defects and other relaxation mechanisms. This frequency dispersion study of our ferroelectric hysteresis loop gives us the confidence that we are measuring the intrinsic switching characteristic of the system and is not dominated by artefacts resulting from leakage and other space charge and other relaxation mechanisms[11, 12]. It was observed that for the device without the ZnO layer (PZT0) the saturation polarization (P_s) is around 35 $\mu C/cm^2$ and the coercive voltages are approximately ± 3 V. In the case of the PZT100 sample the coercive voltages were -9.33 V and 21.55 V respectively for the negative and positive bias. The hysteresis loop opens up with increasing thickness of ZnO, according to Eqn 3.

b) Admittance Angle

To make sure that our measurements are dominated by capacitive contributions we measured admittance angle-voltage characteristics of the PZT sample from 10 kHz-2 MHz **Figure. S5** (b) shows the admittance angles for all the samples for the opposite biases. We can observe that the magnitude of the admittance angle is ~90° at all frequencies. This points to negligible leakage contribution in our samples.

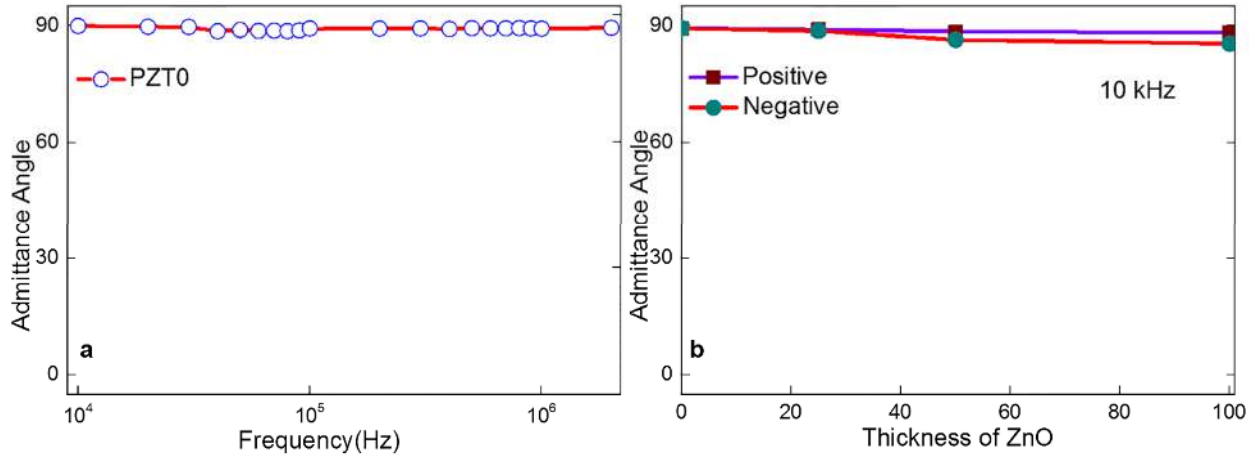

Figure. S5 (a) **Figure. S5** (b)

Figure. S5 (a) The frequency dispersion of the admittance angle between 10 kHz and 2 MHz of the PZT0 sample and (b) Admittance angle of all the samples for opposite biases measured at 10 kHz frequency.

c) Capacitance-Voltage

Capacitance-voltage (C-V) measurements, were anticlockwise for all the samples, and didn't exhibit any signature of a depletion layer, which would lead to an additional series capacitance leading to a decrease in the capacitance for one of the biases[14, 15]. Below, we show the C-V measurements for the PZT0 and PZT25 samples measured at 10 kHz. The arrows denote the direction of voltage sweep.

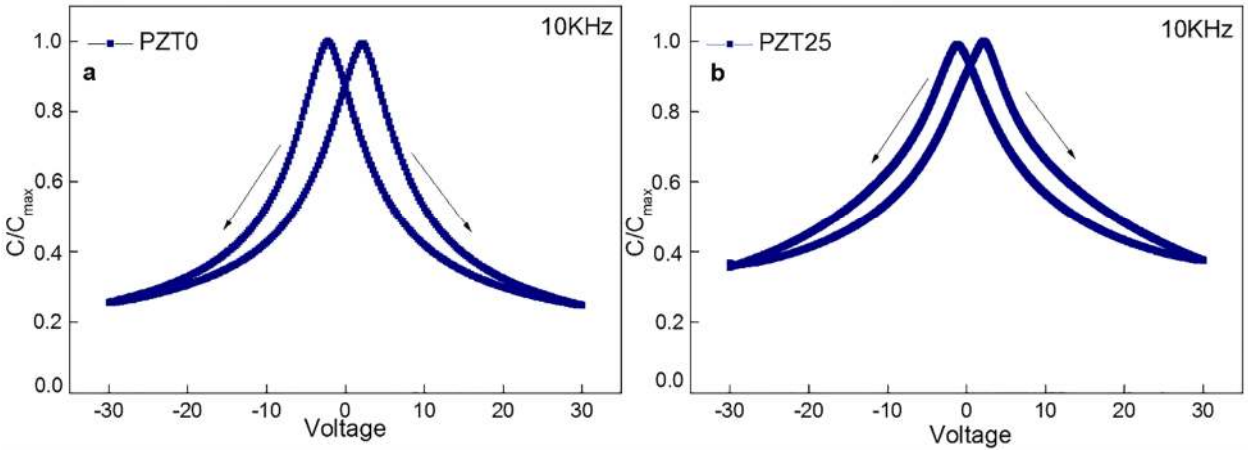

Figure. S6 (a) **Figure. S6** (b)

Figure. S6 C-V characteristics for (a) PZT0 and (b) PZT25 at 10KHz

4. Statistics of local electric field distribution

The wide spectrum of characteristic switching times can be explained by considering the distribution of the local electric fields. We consider the total switching volume as an ensemble of independent switching volumes. These individual switching volumes have individual switching times determined exclusively by the local field. As in earlier works by Tagantsev [16] et al and Genenko [17] et al it is assumed that the switching times have a smooth and exponentially broad distribution. For N different regions with different switching times we can write

$$\Delta P_t/2P_s = \Sigma_{i=0}^{N} (1- \exp [- (t/t_{0i})^n]) \ldots. S1$$

where, t_{0i} is the characteristic switching time corresponding to the i^{th} region. Barthelemy *et al* assumed N=5 in their case [18]. If we assume a broad continuous distribution of switching times $F(logt_0)$ we can write

$$\Delta P_t = 2P_s \int_0^{\infty} \left[1 - \exp\left\{-\left(\frac{t}{t_0}\right)^n\right\}\right] F(logt_0)\, d(logt_0) \quad \ldots. S2$$

From Eqn. 2 because of the one to one relation between the individual switching times and the local electric field we can write $F(logt_0)\, d(logt_0) = F(E)\, d(E)$ …. S3

From Eqn. 1 and Eqn. 2 approximating the double exponential relation between switched polarization and the applied field as a Heaviside step function $\theta[E - E_{th}]$, we can write Eqn. S2 as

$$\Delta P_t = 2P_s \int_0^\infty \theta[E - E_{th}]\, F(E)\, d(E) \;\ldots.\; S4$$

And for statistical normalization

$$\int_0^\infty F(E)\, d(E) = 1 \;\ldots.\; S5$$

The physical meaning of Eqn. S4 is as soon as the applied electric field E exceeds the threshold field E_{th} for a given write time the ferroelectric switches locally. The value of the function $\theta[E - E_{th}] = 0\ for\ E < E_{th}\ and = 1\ for\ E > E_{th}$. As can be seen from Eqn. S4 the functional form of the $F(E)$ can be obtained from the derivative of the $\Delta P_t/2P_s$ as a function of the applied electric field for different write times. In order to maintain switching volume conservation the switching curves which reached the saturation polarization within the maximum possible write time of 1 sec were only fitted.

In **Figure. S7** we show the $\Delta P_t/2P_s$ as a function of the applied electric field for different write times for the PZT50 sample for WDRU (The plots for PZT and WDRU of PZT25 as well as PZT100 have similar characteristics.). Since the data points were scattered we spline fitted the curves which are shown here. As can be seen from **Figure. S7** (a) as the write times decrease the maximum peak voltage increases. The observed plots were found to fit best with Lorentzian distribution functions as compared to a Gaussian. In **Figure. S7** (b) we show the rescaled plots of **Figure. S7** (b) using (E-E_{max})/w where E_{max} is the central maximum value and w is the full width at half maxima. This scaling behaviour suggests that the distribution is intrinsic. A Lorentzian can describe the distribution of horizontal distances at which a line segment tilted at a random angle cuts the x-axis. Similarly, if there exists a singular field (responsible for the growth activation barrier) aligned at a random angle to the domain wall propagation direction its distribution will also be a Lorentzian[19].

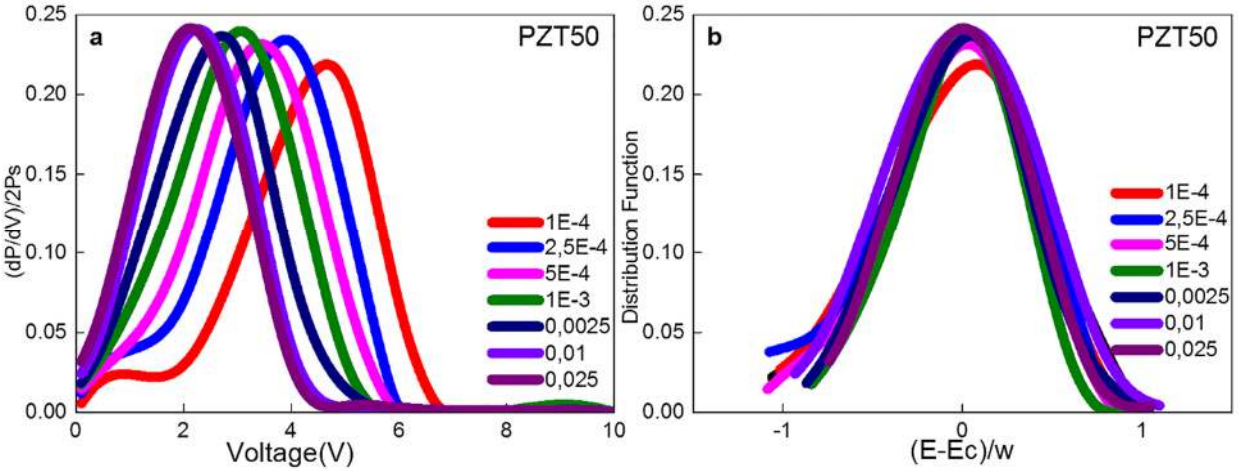

Figure. S7 (a) **Figure. S7** (b)

Figure. S7 (a) Logarithmic derivative of the fractional switched polarization versus applied voltage (b) Normalized distribution of activation field for WDRU for PZT50. All the distributions were found to fit best with a Lorentzian.

Similarly as above in **Figure. S8** we show the $\Delta P_t/2P_s$ as a function of the applied electric field for different write times for the PZT50 sample for WURD. Similar as observed in **Figure. S7** (a) as the write times decrease the maximum peak voltage increases. As we can see from **Figure. S9** (a) the curves don't quite follow any regular shape and also the shape varies with the write time. It signifies that the local fields are not symmetrically distributed about the mean. Since the switching here is governed by the local field variations at the ZnO-PZT interface, which is dependent on the roughness and local disorder the distribution of local electric fields need not necessarily be a singular well defined peak function. In order to rescale these asymmetric curves we use the asymmetric double sigmoid function. Its notable here that Tagantsev et al assumed a mesa like function to map the distribution of characteristic switching times which can qualitatively describe the linear $\Delta P_t/2P_s$ vs write time curve but would not be sufficient to fully map the local electric fields as in our case. As in Eqn. 6 E_{max} is the central value of the derivative and w_1 is the full width at the half maxima and w_2 and w_3 determines the asymmetry of the

distribution in the lower and higher value than E_{max}. We rescale the above curves using $(E-E_{max})/w_1$ which we show in **Figure. S8** (b).

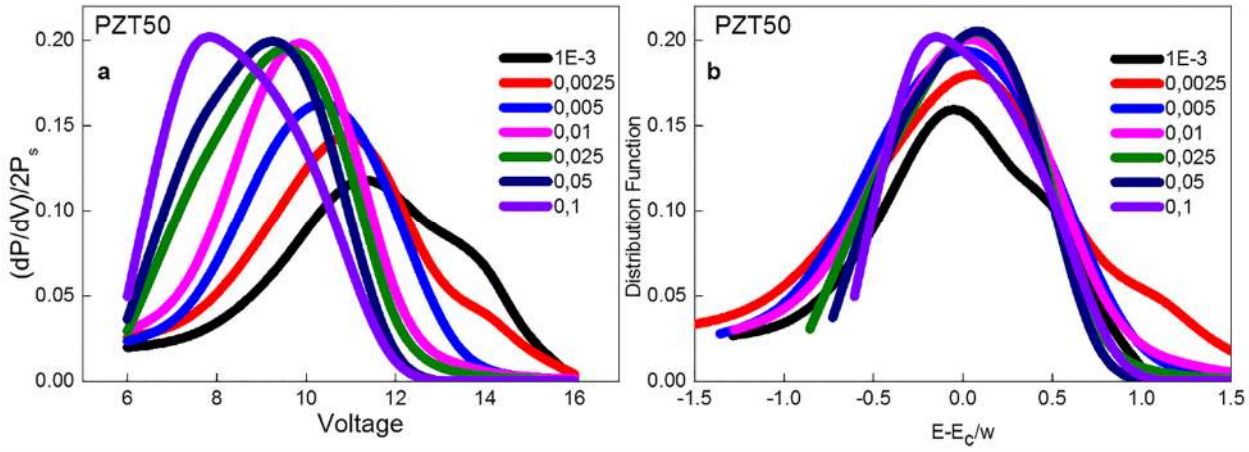

Figure. S8 (a) **Figure. S8** (b)

Figure. S8 (a) Logarithmic derivative of the fractional switched polarization versus applied voltage (b) Normalized distribution of activation field for WURD for PZT50. All the distributions were found to fit best with an asymmetric double sigmoidal function.

5. Retention

The retention of the polarization for all the samples was measured by varying the delay to read time from 10^{-1} - 10^{3} secs as in **Figure. S9**. The switched polarization was found to be stable with less than a 2% drop over the measured time scale for PZT0 and a maximum of 4% drop for PZT100 sample. It shows that the switched polarization is stable over time. Here we plot the retention of the switched polarization as a function of delay to read time from 10^{-1} to 10^{3} secs for all the samples for both the biases. We have studied the retention up to 10^{4} which showed similar trends. As in Figure S9.

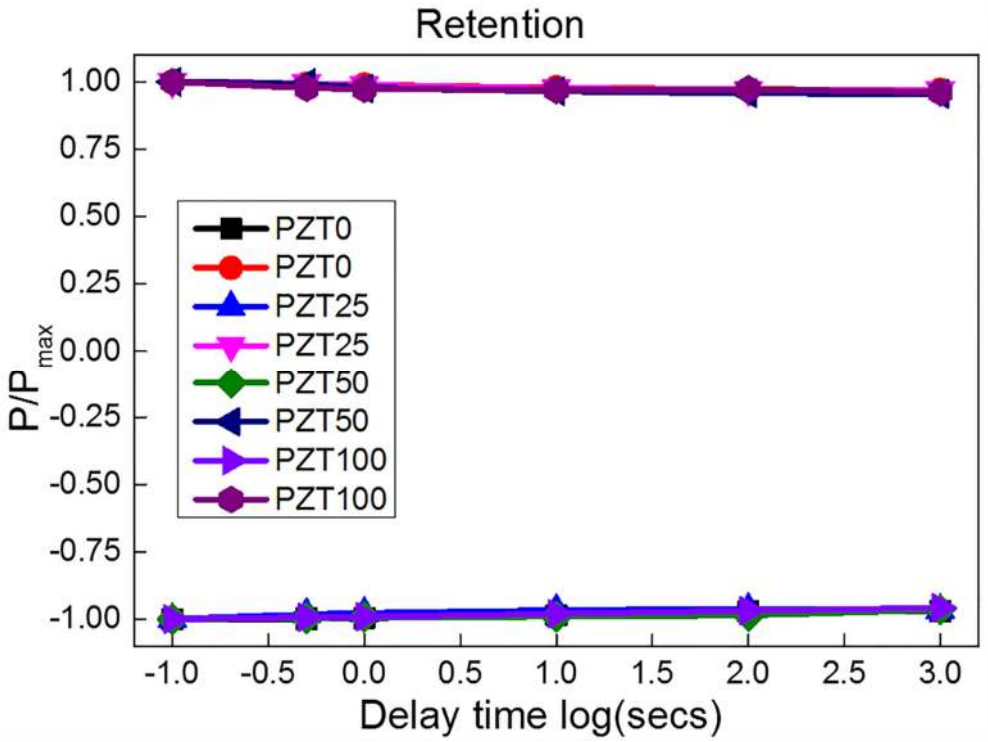

Figure. 9

Figure. S9 Switched polarization as a function of delay to read time.

References

1. S. D. Ha and S. Ramanathan, Journal of Applied Physics **110** (7), 071101 (2011).

2. M. Prezioso, F. Merrikh-Bayat, B. D. Hoskins, G. C. Adam, K. K. Likharev and D. B. Strukov, Nature **521** (7550), 61-64 (2015).

3. J. Schmidhuber, Neural networks : the official journal of the International Neural Network Society **61**, 85-117 (2015).

4. L. P. Shi, K. J. Yi, K. Ramanathan, R. Zhao, N. Ning, D. Ding and T. C. Chong, Applied Physics A **102** (4), 865-875 (2011).

5. S. Dehaene, N. Molko, L. Cohen and A. J. Wilson, Current opinion in neurobiology **14** (2), 218-224 (2004).

6. T. Knight, and George Stiny, Arq: architectural research quarterly **5.04**, 355 (2001).

7. J. M. Zurada, St. Paul: West, (1992.).

8. D. kriesel, **2011** (August 15 (2007): .).

9. S. Song, Kenneth D. Miller, and Larry F. Abbott, Nature neuroscience **3.9**, 919-926 (2000).

10. L. F. Abbott, and Sacha B. Nelson, Nature neuroscience **3**, 1178-1183. (2000).

11. L. Pintilie and M. Alexe, Applied Physics Letters **87** (11), 112903 (2005).

12. J. F. Scott, *Ferroelectric memories*. (Springer Science & Business Media, 2000).

13. J. F. Scott, Journal of Physics: Condensed Matter **20** (2), 021001 (2008).

14. W. Choi, S. Kim, Y. W. Jin, S. Y. Lee and T. D. Sands, Applied Physics Letters **98** (10), 102901 (2011).

15. I. Pintilie, I. Pasuk, G. Ibanescu, R. Negrea, C. Chirila, E. Vasile and L. Pintilie, Journal of Applied Physics **112** (10), 104103 (2012).

16. A. K. Tagantsev, I. Stolichnov, N. Setter, J. S. Cross and M. Tsukada, Physical Review B **66** (21) (2002).

17. S. Zhukov, Y. A. Genenko and H. von Seggern, Journal of Applied Physics **108** (1), 014106 (2010).

18. A. Chanthbouala, V. Garcia, R. O. Cherifi, K. Bouzehouane, S. Fusil, X. Moya, S. Xavier, H. Yamada, C. Deranlot, N. D. Mathur, M. Bibes, A. Barthelemy and J. Grollier, Nature materials **11** (10), 860-864 (2012).

19. E. W. Weisstein, (Mathematica, From MathWorld A Wolfram Web Resource).